Journal Pre-proofs

Motion of a friction belt drive at mixed kinematic description

Jakob Scheidl

PII: S0020-7683(20)30168-2
DOI: https://doi.org/10.1016/j.ijsolstr.2020.05.001
Reference: SAS 10704

To appear in: *International Journal of Solids and Structures*

Received Date: 16 December 2019
Revised Date: 30 April 2020
Accepted Date: 2 May 2020

Please cite this article as: J. Scheidl, Motion of a friction belt drive at mixed kinematic description, *International Journal of Solids and Structures* (2020), doi: https://doi.org/10.1016/j.ijsolstr.2020.05.001

This is a PDF file of an article that has undergone enhancements after acceptance, such as the addition of a cover page and metadata, and formatting for readability, but it is not yet the definitive version of record. This version will undergo additional copyediting, typesetting and review before it is published in its final form, but we are providing this version to give early visibility of the article. Please note that, during the production process, errors may be discovered which could affect the content, and all legal disclaimers that apply to the journal pertain.

© 2020 Published by Elsevier Ltd.

Journal Pre-proofs

Motion of a friction belt drive at mixed kinematic description

Jakob Scheidl

Institute of Mechanics and Mechatronics, TU Wien
Getreidemarkt 9, A-1060 Vienna, Austria
Jakob.Scheidl@tuwien.ac.at

Abstract

The planar problem of a two-pulley belt drive is revisited with account for large transverse deflections due to gravity and frictional contact between the pulleys and the belt, which is modelled as an extensible string. An existing mixed Eulerian–Lagrangian finite element model is extended to simulate the quasistatic, non-stationary motion of the system, where the method of augmented Lagrangian multipliers is adopted for contact treatment, which relies on the penalty regularisation to iteratively update the contact tractions. To validate the numerical results, a semi-analytic solution of the steady state is developed based on belt creep theory. In a comparative study numerical and semi-analytic steady state solutions are verified. The transient evolution of the contact state during quasistatic, non-stationary motion is studied with the finite element scheme.

Keywords: Belt drive mechanics, Mixed Eulerian Lagrangian kinematics, Structural finite elements, Belt creep theory, Dry friction contact

1. Introduction

From the standpoint of structural mechanics axially moving structures are peculiar systems, because the governing equations are readily available in Lagrangian description, but constraints are imposed at fixed points in

Journal Pre-proofs

Journal Pre-proofs

space rather than at material points. Closed loop belt drive systems are an important sub-category of axially moving structures and find widespread use in numerous applications.

Here, we revisit the benchmark problem of a two-pulley belt drive, previously considered in [26], and further extend the therein proposed mixed Eulerian–Lagrangian (abbreviated as E.L. in the following) finite element framework. In contrast to conventional Lagrangian finite element methods, these elements feature a spatial parametrisation of field variables utilizing a geometric contour coordinate. The corresponding finite element nodes then reside at fixed points of this spatial coordinate and may only move in the transverse direction, while material particles keep travelling through the mesh in axial direction. This mixed kinematic description resembles arbitrary Lagrangian–Eulerian formulations (ALE), which are for example traditionally used in the simulation of metal forming processes [21]. Contrary to classic ALE strategies the E.L.-approach avoids frequent re-meshing by direct treatment of the problem in the mixed coordinate domain. Note that the idea of deformable Eulerian meshes has also proven to be efficient in the analysis of fluid-structure interactions [7].

Pure material type finite element formulations are still applicable [4, 12], but constraints then have to be imposed at travelling material points, which induces numerical difficulties. See [15] for a comparative study of mixed versus classic finite element formulations on the example of the quasistatic transient motion of a simple two-pulley belt drive, or [20] for a comparison of different finite element strategies by means of the so called sliding spaghetti problem.

In recent years, the mixed kinematic formulation has been frequently applied in the construction of finite elements for axially moving beams or strings [16, 23] and extensions to axially moving plates are available as well [21, 24]. Contrary to [15], where transverse deformations and bending stiffness were disregarded, the finite element model first reported in [26] deals with large

Journal Pre-proofs

deflections of a possibly slackly mounted belt on two rigid pulleys in the field of gravity with account of both axial and bending stiffness. The presented solutions were however limited to the frictionless, static problem of the belt hanging on the two pulleys. In an effort to extend this formulation, the current contribution aims to simulate the time evolution of motion. Following a simple time stepping strategy the belt is carried from the previously obtained, frictionless equilibrium over to a steady state, for which the spatial configuration of the moving belt remains unchanged, while material particles keep travelling through this stationary deflected state. The discrete sequence of intermediate states then represents the transition process from the initial static equilibrium to the final steady state motion.

The pulley angular velocities are prescribed, which is convenient in the displacement-based finite element framework, and the time evolution is modelled as a quasistatic process that ignores non-stationary inertia effects. Hence, full dynamics of the problem are out of the scope of the present contribution and we refer to [11] for a study of small perturbations of the stationary motion as well as [25], which considers transient motion of a simple belt drive with an idealised friction model. Moreover, see [22] and the more recent study [6] for stability analyses of axially moving structures.

The frictional contact of solids remains an important research topic concerned with both the development of appropriate theoretical models [13] as well as their consistent implementation in numerical schemes [17, 28]. Here, we assume Coulomb dry friction for the power transmission and refer to [9] for an alternative treatment utilizing a spring-damper model. The consistent account for distributed frictional contact in the mixed finite element framework is a novel result. The contact state is resolved discretely at individual integration points, which allows for an unrestricted development of distinct stick and slip zones in the course of motion. The corresponding constraints are enforced by means of the so-called method of augmented Lagrange multipliers [19], which relies on the penalty regularisation method to iteratively

Journal Pre-proofs

update Lagrange multiplier estimates for the contact forces. As previously reported in [26], this strategy cannot be used in problems with bending stiffness, which is why we return to the simpler model of an extensible string for the belt in the present contribution.

In addition to the finite element treatment of the benchmark example, in Section 3 we propose a novel semi-analytic strategy designed to compute the steady state solution of the same problem. Using numerical integration routines we obtain practically converged results that serve as reference values in the comparison to stationary finite element solutions. Similar derivations and solution strategies corresponding to the creep-theory of an extensible string can be found in the literature. An exact solution for the steady motion of an extensible string, which is easily extendable to multi-pulley belt drive systems is presented in [18]. The effect of bending stiffness on the steady motion problem of a two-pulley belt drive is studied in [10]. However, the authors of the last reference employ certain simplifications, which lead to string-like equations in the contact regions and effectively alleviate the provision for bending effects. Here, we disregard bending effects completely and, contrary to the above references, take gravity into account. This extension allows for large transverse deflections in the string model, which are absent in traditional studies [1, 18] that focus on power transmission problems. However, inclusion of gravity is essential when simulating slackly mounted structures such as: steel conveyor belts, timing belts or cable cars; see also [3], which studies the setting of a shear-deformable belt on two pulleys with emphasis on the influence of gravity.

2. Mixed Eulerian–Lagrangian finite element procedure

We revisit the problem of a simple two-pulley belt drive, depicted in Figure 1. The belt is modelled as an extensible string. The pulleys' centre to centre distance is H, both have the same radius R, but may rotate with different constant angular velocities ω_1 and ω_2. In addition the gravitational

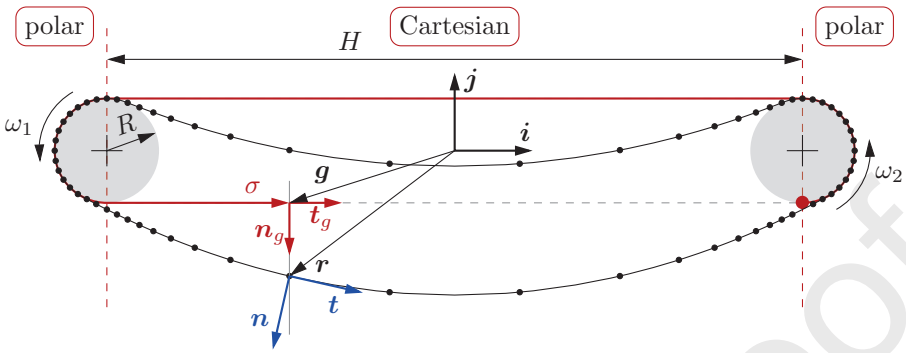

Figure 1: Finite element model; mixed finite element mesh and spatial parametrisation of the position vector $\boldsymbol{r}$ in the compound coordinate σ

force acts downwards in opposite direction of $\boldsymbol{j}$, which is part of the fixed Cartesian system $[\boldsymbol{i}, \boldsymbol{j}]$.

The picture further illustrates the mixed Eulerian–Lagrangian description that utilizes the compound spatial coordinate σ for parametrisation of the position vector $\boldsymbol{r}$. The planar basis $[\boldsymbol{t}, \boldsymbol{n}]$ rotates with $\boldsymbol{r}$ just like the basis $[\boldsymbol{t}_g, \boldsymbol{n}_g]$ does with the vector $\boldsymbol{g}$, which traces the circumference of σ. The mixed kinematic description prohibits axial motion of finite element nodal points and thus, contrary to conventional finite elements, enables locally refined meshes, such as the one shown in Figure 1.

As a consequence of the quasistatic strategy, the explicit time dependence of unknowns may be ignored in most circumstances. However, treating tangential contact kinematics with velocities rather than finite differences is more concise and insightful. For this reason, we will formally consider variables to be time dependent.

2.1. Variational form and energy contributions

In the time-discretised framework the solution for a single time step corresponds to a stationary point of the Lagrangian L:

$$\delta L = \delta U + \delta V_{\text{gravity}} + \delta V_{\text{contact}} - \delta T = 0\,, \tag{1}$$

Journal Pre-proofs

which involves the strain energy U, the gravity potential V_{gravity}, the contact potential V_{contact} as well as the kinetic energy T. Note that (1) is a direct consequence of Hamilton's principle applied for quasistatic processes, see also [9, 27]. In general, we seek the time evolution of motion as a sequence of solutions to (1). In this regard, the limitation to a quasistatic treatment means that we cannot account for full transient dynamics. More precisely, only such inertia contributions that persist in the stationary state can be included and are contained in the term δT. As it is not meaningful to account for only this part of inertia effects when simulating the transient process, we distinguish between two kinds of finite element analyses:

- FES_0: finite element simulation of the transient process that approaches a steady state with full disregard of inertia contributions ($\delta T = 0$),
- FES_T: finite element simulation with inclusion of δT seeking just the corresponding stationary solution.

In both cases the same time-stepping strategy is used. However, for FES_0 the obtained time sequence of states has a physical meaning, whereas for FES_T the time t merely plays the role of a homotopy parameter in an iteration procedure for the steady state solution.

Any one of the energies introduced in (1) is written as an integral with respect to the material arc coordinate $s \in [0,\, s_{\max}]$ of the rod. The contact potential will be covered later in Subsection 2.3 and the other contributions are

$$U = \int_0^{s_{\max}} \frac{b}{2}\,\epsilon^2 \,\mathrm{d}s\,, \quad V_{\text{gravity}} = \int_0^{s_{\max}} G\,y \,\mathrm{d}s\,, \quad T = \frac{1}{2}\int_0^{s_{\max}} \boldsymbol{v}\cdot\boldsymbol{v}\,\rho \,\mathrm{d}s\,. \tag{2}$$

In the latter two formulas the specific gravitational force $G = \rho\, g$, as mass per unit material length ρ times gravitational constant g, the vertical coordinate of a material point y and the material velocity $\boldsymbol{v}$ appear. The elastic strain energy U of the extensible string depends on the Green axial strain ϵ with

a corresponding stiffness coefficient b. We introduce a shorthand for the material derivatives $\partial_s(\ldots) = \partial(\ldots)/\partial s$ to formulate the strain relation

$$\epsilon = \frac{1}{2}\left(\partial_s \boldsymbol{r} \cdot \partial_s \boldsymbol{r} - 1\right) . \tag{3}$$

Consequently, the finite element formulation needs to at least ensure continuity of first order derivatives $\partial_s \boldsymbol{r}$. To fulfil this requirement in the compound coordinate regime of σ, we have to employ nonlinear finite element approximations in the degrees of freedom, see [26].

In the E.L.-framework the spatial coordinate $\sigma \in [0,\, \sigma_{\max}]$ parametrises the material line by means of a suitable transformation $s = s\,(\sigma,\, t)$. Corresponding mixed finite elements typically make use of an additional transformation $\sigma = \sigma\,(\xi)$ to a local coordinate $\xi \in [-1,\, 1]$. The total energies are then obtained through summation over finite element contributions. The transformation steps of a single integral quantity to the finite element model can thus be written as

$$E = \int_0^{s_{\max}} e\,(s,t)\ \mathrm{d}s = \int_0^{\sigma_{\max}} e\,(\sigma,t)\ \partial_\sigma s\ \mathrm{d}\sigma = \sum_{\mathrm{el}} \int_{-1}^{1} e\,(\xi,t)\ \partial_\sigma s\, \partial_\xi \sigma\ \mathrm{d}\xi\,, \tag{4}$$

where e serves as a placeholder for the material density of a single energy component $E = \{U,\, V_{\mathrm{gravity}},\, V_{\mathrm{contact}},\, T\}$ in different descriptions. The integration ranges $s_{\max}$ and $\sigma_{\max}$ denote the total material and geometric lengths, respectively. The element-wise integrals are computed using Gauss-quadrature formulas with three integration points.

For numerical solution of equation (1) we adopt a pure Newton-Raphson algorithm that relies on the linearisation of δL with respect to the finite element nodal unknowns. Although analytical derivation of second order derivatives of L is still manageable for the problem at hand, they are more conveniently approximated numerically using finite differences.

2.2. Mixed finite element kinematics

We refer to [26] for an elaborate discussion on the adopted mixed finite element kinematics and here repeat some important features. As illustrated in Figure 1, the position vector may be written in the form

$$\boldsymbol{r}\left(\sigma,\, t\right) = \boldsymbol{g}\left(\sigma\right) + \nu\left(\sigma,\, t\right)\, \boldsymbol{n}_{\mathrm{g}}\left(\sigma\right)\,. \tag{5}$$

Aside from the spatial contour coordinate σ, we further introduce a transverse coordinate ν that represents the distance of a given point from the line $\boldsymbol{g}$ in direction $\boldsymbol{n}_{\mathrm{g}}$. Since we are parametrising a one-dimensional, material line the transverse displacement itself needs to be treated as a function of the axial coordinate $\nu = \nu\left(\sigma,\, t\right)$.

In order to follow the movement of a particular material point s in the E.L.-formulation, the material coordinate becomes an additional unknown, which can be obtained indirectly by means of a material displacement $\bar{s}$ as

$$s\left(\sigma,\, t\right) = \lambda\,\left(\sigma + \bar{s}\left(\sigma,\, t\right)\right)\,. \tag{6}$$

Here, $\lambda = s_{\max}/\sigma_{\max}$ is defined as the ratio of total lengths meaning that $\lambda > 1$ corresponds to slackly spanned belts with presumably large deformations, whereas $\lambda < 1$ indicates greater pre-tension and smaller deflections. In the above equation λ just compensates for the different coordinate lengths of σ and s. By avoidance of using the material coordinate s directly as an unknown, it is easy to treat the looping condition at the endless belt connecting point where s and σ experience jumps by $s_{\max}$ and $\sigma_{\max}$, but $\bar{s}$ remains continuous with $\bar{s}\left(0,\, t\right) = \bar{s}\left(\sigma_{\max},\, t\right)$.

We now aim to compute the sliding velocity (or the relative displacement u in a time discretised sense), which is the main kinematic quantity that characterises the frictional behaviour of a given integration point. In this regard, we introduce shorthands for the material (total) and the spatial (local)

Journal Pre-proofs

time derivative

$$\mathring{\partial}_t (\dots) = \left.\frac{\partial (\dots)}{\partial t}\right|_{s=\text{const}} , \quad \partial_t = \left.\frac{\partial (\dots)}{\partial t}\right|_{\sigma=\text{const}} , \tag{7}$$

and state that the total time derivative of the material coordinate $s = s(\sigma, t)$ is zero

$$\mathring{\partial}_t s = \partial_t s + \partial_\sigma s \, \mathring{\partial}_t \sigma = 0 . \tag{8}$$

The material particle velocity follows to

$$\mathring{\partial}_t \boldsymbol{r} = \boldsymbol{v} = \boldsymbol{t}_\mathrm{g} \, (1 + \alpha \, \nu) \, \mathring{\partial}_t \sigma + \boldsymbol{n}_\mathrm{g} \, \mathring{\partial}_t \nu , \tag{9}$$

where α represents the absolute value of the non-smooth derivative of the normal vector $\boldsymbol{n}_\mathrm{g}$ defined as

$$\alpha = |\partial_\sigma \boldsymbol{n}_\mathrm{g}| = \begin{cases} 0 & \dots \text{ Cartesian region of } \sigma \\ 1/R & \dots \text{ polar region of } \sigma \end{cases} . \tag{10}$$

It enables simultaneous treatment of the entire domain of σ using (9). Any point in contact at the beginning of a step is presumed to remain in contact. Therefore, the material velocity in outward pointing normal direction $\boldsymbol{n}$ of a point on the pulley surface has to vanish. We recall $\boldsymbol{v}$ from (9) and project onto the local basis vectors $\{\boldsymbol{t}, \boldsymbol{n}\}$

$$\boldsymbol{v} \cdot \boldsymbol{t} = \boldsymbol{t}_\mathrm{g} \cdot \boldsymbol{t} \, (1 + \alpha \, \nu) \, \mathring{\partial}_t \sigma + \boldsymbol{n}_\mathrm{g} \cdot \boldsymbol{t} \, \mathring{\partial}_t \nu \tag{11a}$$

$$\boldsymbol{v} \cdot \boldsymbol{n} = \boldsymbol{t}_\mathrm{g} \cdot \boldsymbol{n} \, (1 + \alpha \, \nu) \, \mathring{\partial}_t \sigma + \boldsymbol{n}_\mathrm{g} \cdot \boldsymbol{n} \, \mathring{\partial}_t \nu = 0 . \tag{11b}$$

We use the second equation to substitute $\mathring{\partial}_t \nu$ in the first one and, after some transformations, end up with

$$\boldsymbol{v} \cdot \boldsymbol{t} = \frac{(1 + \alpha \, \nu) \, \mathring{\partial}_t \sigma}{\boldsymbol{n}_\mathrm{g} \cdot \boldsymbol{n}} . \tag{12}$$

Journal Pre-proofs

If we assume a sufficiently large penalty factor for normal contact, the radial displacement ν practically vanishes in the polar domain. Moreover, $\alpha = 0$ holds in the Cartesian regime and the above relation further simplifies to

$$\boldsymbol{v} \cdot \boldsymbol{t} = \frac{-\partial_t s}{\partial_\sigma s \, (\boldsymbol{n}_\mathrm{g} \cdot \boldsymbol{n})} \,, \tag{13}$$

with $\mathring{\partial}_t \sigma = -\partial_t s / \partial_\sigma s$ according to (8). Now, computation of the sliding velocity $\partial_t u$ is a simple matter of subtraction with the tangential velocity of the corresponding pulley

$$\partial_t u = \frac{\partial_t s}{\partial_\sigma s \, (\boldsymbol{n}_\mathrm{g} \cdot \boldsymbol{n})} - R \, \omega \,, \tag{14}$$

where the appropriate angular velocity $\omega = \{\omega_1, \, \omega_2\}$ has to be inserted. Finally, direct time discretization of local time derivatives with a finite time step Δt results in the tangential relative displacement

$$u = \frac{\Delta s}{\partial_\sigma s \, (\boldsymbol{n}_\mathrm{g} \cdot \boldsymbol{n})} - R \, \omega \, \Delta t \,. \tag{15}$$

The material coordinate increment Δs and $\partial_\sigma s$ may be easily described as functions of the nodal unknowns and the dot-product of normal vectors depends on σ alone, provided that the belt is congruent with the outer contour of the pulley.

The following remark solely applies to finite element simulations of the type FES_T, and is also significant for the semi-analytic treatment of stationary motion in Section 3: For the special case of steady state motion the main kinematic unknowns take the form

$$\nu = \nu \, (\sigma) \;, \quad s \, (\sigma, \, t) = S \, (\sigma) + c \, t \,. \tag{16}$$

These conditions ensure that the spatial configuration of the belt remains fixed with $\boldsymbol{r} = \boldsymbol{r} \, (\sigma)$, while material is transported through this stationary

Journal Pre-proofs

deflected state at a constant rate $\partial_t s = \text{const} = c$. The particular distribution of material particles $S(\sigma)$ along the deformed line does not change with respect to time and neither do the strains as a consequence. These characteristics of steady state motion are emphasized in the literature [5, 14] and the second condition of (16) is sometimes used to perform a coordinate transformation [18]. With the above relation (8) for $\mathring{\partial}_t \sigma$ the velocity for the stationary state becomes

$$\boldsymbol{v} = \frac{-c}{\partial_\sigma S} \left[\boldsymbol{t}_\mathrm{g} \left(1 + \alpha\, \nu\right) + \boldsymbol{n}_\mathrm{g}\, \partial_\sigma \nu \right] . \tag{17}$$

In particular, the spatial time derivative $\partial_t \nu$ vanishes in this case. As we are merely interested in the steady state solution when performing a FES_T analysis, it is sufficient to use the above simplified formula to evaluate the kinetic energy. However, since c and $\partial_\sigma S(\sigma)$ are attributes of the stationary state and thus not known in advance, we need to provide approximations. For $\partial_\sigma S(\sigma)$ we simply take the latest result and for c the arithmetic mean of all integration point velocities is used

$$\partial_\sigma S(\sigma) \approx \partial_\sigma s(\sigma,\, t) , \quad c \approx \frac{1}{3\, N_\mathrm{el}} \left(\sum_{\mathrm{el}} \sum_{i=1}^{3} \partial_t s(\xi_i,\, t) \right) , \tag{18}$$

where N_el denotes the number of elements in the model and ξ_i are the local integration point coordinates with a total of three per element. Both approximations approach their final results as the time integration progresses.

2.3. Contact modelling

This section covers the novel implementation of Coulomb dry friction contact in the existing mixed finite element framework. The pulleys are treated as rigid, analytical bodies, i.e. the contact pairing is rigid body with deformable structure. In general, solid body contacts may be formulated as constrained variational problems or variational inequalities. The accompanying constraints are the impenetrability condition and the Coulomb friction

Journal Pre-proofs

Journal Pre-proofs

criterion, which may be written in the form of Kuhn-Tucker conditions, see [19, 28]. The impenetrability condition ensures that the deformable body may never penetrate the rigid counterpart. In the present case this requires the penetration depth of the belt into the pulley to remain zero; $\gamma = 0$. Moreover, the Coulomb criterion requires the friction state to reside within or at most on the friction cone; formally expressed as

$$\Phi = |\tau_\perp| - \mu\,\tau_\mathrm{N} \leq 0\,. \tag{19}$$

It compares the absolute value of the tangential tractions $\tau_\perp$ to the maximum transferable friction force given as a product of normal contact pressure and friction coefficient μ, which is used for both sliding and sticking friction. Naturally, for sliding friction $\Phi = 0$ holds and for sticking $\Phi < 0$ applies.

Traditionally, these contact constraints are accounted for either by introduction of Lagrange multipliers or via a penalty regularisation strategy. The here proposed scheme originates from a proper combination of both strategies also known as augmented Lagrangian multiplier method, see [19]. Basically, it aims to solve the Lagrangian multiplier problem through iterative solution of the simpler-to-solve penalty regularisation equivalent.

In the present context, proper contact treatment requires definition of contact penalty potentials and contact state update procedures. The potentials are needed to compute contributions to the system of equations during a Newton iteration, whereas the update scheme specifies how to adapt the contact state based on the solution data available. To accomplish these tasks, we first need to specify both contact tractions in the non-material finite element model: For the pure penalty approach, the impenetrability constraint is no longer strictly enforced, but rather approximated by punishing any penetration γ of the belt into the pulley surface with a high factor P_N. This idea is modified just slightly in the augmented Lagrangian approach

$$\tau_\mathrm{N} = \lambda_\mathrm{N} + P_\mathrm{N}\,\gamma \geq 0\,. \tag{20}$$

Here λ_N stands for the present Lagrange multiplier estimate and $P_\mathrm{N}\,\gamma$ is the classic penalty part. Naturally, the normal contact pressure is strictly positive, and any point that produces a negative result is not in contact at all. This also implies that even negative values of the penetration depth have to be considered, which correspond to the belt lifting off of the pulley surface just slightly, such that (20) remains positive. The update procedure in the sense of the augmented strategy is a simple fixpoint iteration scheme

$$\lambda_\mathrm{N} \leftarrow \lambda_\mathrm{N} + P_\mathrm{N}\,\gamma\,. \tag{21}$$

Upon convergence the penetration depth γ vanishes at which point the Lagrange multiplier estimate becomes exact.

The implementation of the augmented scheme for frictional contact is more complicated as it has to deal with both sliding and sticking states, yet the basic expression for the tangential traction is equally simple

$$\tau_\perp^* = \lambda_\perp + P_\perp\,u\,. \tag{22}$$

The Lagrange multiplier estimator for frictional contact is $\lambda_\perp$ and the penalty component consists of another penalty stiffness $P_\perp$ and the relative, tangential displacement u according to (15). We call $\tau_\perp^*$ the auxiliary traction, because its purpose is threefold. Firstly, it is used to evaluate the Coulomb friction criterion Φ, replacing $\tau_\perp$ in (19), to determine a point's frictional contact state. Secondly, it equals the actual tangential traction in case of stick, formally written as $\tau_\perp|_\mathrm{stick} = \tau_\perp^*$. And lastly, it defines the sliding direction in case of slipping motion

$$e = \frac{\tau_\perp^*}{|\tau_\perp^*|} = \pm 1\,, \tag{23}$$

where $e = +1$ indicates forward sliding, meaning that belt points overtake their counterparts on the pulley surface, and $e = -1$ corresponds to sliding in

Journal Pre-proofs

	normal contact	sticking friction	sliding friction
criterion	$\lambda_\mathrm{N} + P_\mathrm{N}\,\gamma > 0$	$\Phi < 0$	$\Phi \geq 0$
actual traction	$\tau_\mathrm{N} = \lambda_\mathrm{N} + P_\mathrm{N}\,\gamma$	$\tau_\perp = \tau_\perp^*$	$\tau_\perp = e\,\mu\,\tau_\mathrm{N}$
update procedure	$\lambda_\mathrm{N} \leftarrow \tau_\mathrm{N}$	$\lambda_\perp \leftarrow \tau_\perp$	
with: $\tau_\perp^* = \lambda_\perp + P_\perp u\,, \quad \Phi = \lvert\tau_\perp^*\rvert - \mu\,\tau_\mathrm{N}\,, \quad e = \frac{\tau_\perp^*}{\lvert\tau_\perp^*\rvert}$			

Table 1: Augmented Lagrangian treatment of contacts; contact state criteria, actual traction values and update routines

opposite direction.[1] Having deduced the direction of relative movement the sliding tangential traction becomes $\tau_\perp|_\mathrm{slip} = e\,\mu\,\tau_\mathrm{N}$. This measure guarantees that sliding friction states indeed reside on the friction cone $\Phi = 0$, whereas evaluation of Φ with the auxiliary traction $\tau_\perp^*$ may even produce results $\Phi > 0$, failing the Coulomb criterion. Hence, a point is considered sticking if evaluation of (19) with $\tau_\perp^*$ leads to $\Phi < 0$ and treated as slipping if $\Phi \geq 0$ holds. In analogy to (21) we define another iterative update scheme for the Lagrange multiplier estimate $\lambda_\perp$

$$\lambda_\perp \leftarrow \tau_\perp \quad \text{with} \quad \tau_\perp|_\mathrm{stick} = \tau_\perp^*\,, \quad \tau_\perp|_\mathrm{slip} = e\,\mu\,\tau_\mathrm{N}\,. \tag{24}$$

The whole augmented Lagrangian procedure for both normal and frictional contact is summarised in Table 1, featuring the contact state criteria, the computation of tractions and the update procedures for Lagrange multiplier estimates.

[1] It is worth noting that calling $\tau_\perp^*$ and all its relatives "tangential tractions" is somewhat misleading from a physical standpoint, because the real tractions always act in opposite direction of the relative motion. Here, as (23) suggests, the so-called tangential tractions and the sliding velocities point in the same direction.

The contact state is resolved discretely at Gaussian integration points in the finite element model and consequently a corresponding set of contact data is stored for every single point: We need to keep track of the Lagrange multiplier estimates λ_{N} and $\lambda_{\perp}$. In addition, the current value of Φ is memorised as a contact state identifier. The contact state update procedures are invoked once per time step.

To conclude the derivation it remains to specify the contact penalty potential V_{contact}, whose variation can be split into two contributions, one attributed to the normal contact forces and one to the friction forces

$$\delta V_{\mathrm{N}} = \int_0^{s_{\max}} \tau_{\mathrm{N}}\, \mathring{\delta}\gamma \, \mathrm{d}s\,, \quad \delta V_{\perp} = \int_0^{s_{\max}} \tau_{\perp}\, \mathring{\delta} u \, \mathrm{d}s\,, \tag{25}$$

where we have introduced the material variation operator $\mathring{\delta}$ in analogy to the total time derivative (7) to emphasize that γ and u are to be varied at fixed material coordinates s; see [23] for an in-depth discussion on the topic of total and local variations of fields. For it to equal the just introduced variational form, the normal contact potential must read

$$V_{\mathrm{N}} = \int_0^{s_{\max}} \left(\lambda_{\mathrm{N}}\, \gamma + \frac{1}{2}\, P_{\mathrm{N}}\, \gamma^2 \right) \mathrm{d}s\,, \tag{26}$$

which is a simple extension of the pure penalty version presented in [26]. Analogously, the friction potential in case of stick reads

$$V_{\perp,\mathrm{stick}} = \int_0^{s_{\max}} \left(\lambda_{\perp}\, u + \frac{1}{2}\, P_{\perp}\, u^2 \right) \mathrm{d}s\,, \tag{27}$$

but the expression for the sliding potential is less obvious

$$V_{\perp,\,\mathrm{slip}} = \int_0^{s_{\max}} \frac{\mu\, \tau_{\mathrm{N}}}{P_{\perp}}\, |\tau_{\perp}^{*}| \, \mathrm{d}s\,. \tag{28}$$

Its rather complicated appearance is a consequence of the fact that the sliding

Journal Pre-proofs

Journal Pre-proofs

direction e is not prescribed. To show the equivalence with (25) one merely needs to compute the variation of the above formula. The usual integral transformation rules (4) apply to the just introduced components of the contact potential.

3. Semi-analytical treatment of stationary motion

In order to validate the finite element results, we derive and integrate a boundary value problem for the belt drive at steady state motion. We revisit belt creep theory with the usual prerequisites, namely: We assume Coulomb friction in the contact regimes and model the belt as an extensible string. Stationary inertia effects are considered.

The deduced boundary value problem is similar to those reported in [10] and [18] with the exception that gravity is taken into account. Furthermore, not the geometric arc coordinate, but a Cartesian spatial coordinate x is used for parametrisation in the free span region, see Figure 2, which is closely related to the one used in the finite element model, compare Figure 1.

We recall that, in accordance with (16), the sought for steady state motion is characterized by a "frozen" deformation state through which material particles are transported at a constant rate $\partial_t s = c$, which is to be determined as part of the solution. The boundary conditions for the whole system may be categorised into numerous, local matching conditions and a single, global closing condition. The latter, which may also be denoted as looping condition, demands that the total material length of the whole belt equals the specified one, namely $s_{\max}$. Now, in an effort to ease the solution process we first disregard the closing condition, which enables us to prescribe the material transport rate c as an additional parameter and, more importantly, allows to divide the whole boundary value problem into individually solvable sub-problems. Later, we can iteratively fulfil the remaining closing condition by means of a root problem for the correct value of c and thereby obtain the steady state solution of the complete belt drive. This procedure is eas-

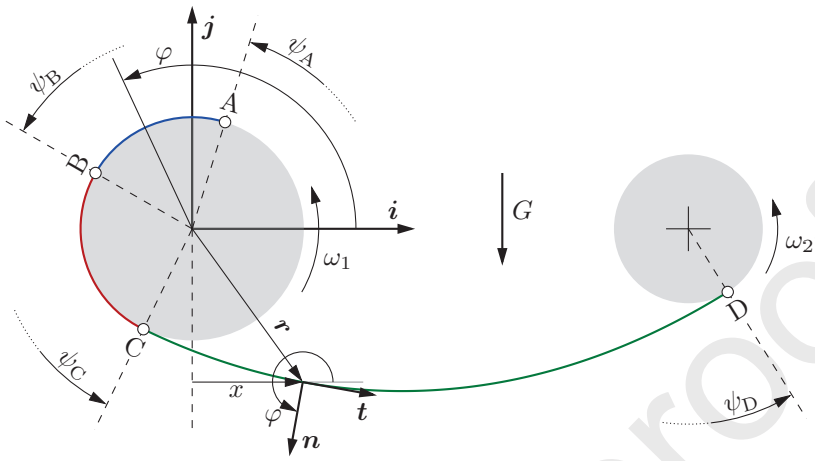

Figure 2: Semi-analytical model for a single belt segment consisting of one sticking $\overline{\mathrm{AB}}$, one sliding $\overline{\mathrm{BC}}$ and one free span region $\overline{\mathrm{CD}}$; Cartesian reference frame $[\boldsymbol{i}, \boldsymbol{j}]$; piecewise spatial parametrisation with the coordinates φ and x

ily extendible to multi-pulley belt drives and we refer to [10, 18] for similar strategies.

The method is demonstrated on the example of a two-pulley drive and we begin by dividing the closed belt into two individual segments. The first segment consists of the left pulley contact region and the lower free span, whereas the second one comprises the right pulley contact zone and the upper free span. Since governing equations and boundary conditions for both segments look alike, it is sufficient to focus on a single one, and thus only the first segment is depicted in Figure 2. We further distinguish three distinct regions of this segment: one sticking $\overline{\mathrm{AB}}$, one sliding $\overline{\mathrm{BC}}$ and one free span region $\overline{\mathrm{CD}}$. To make the formulation more suitable for multi-pulley drives, the pulleys may now have different radii R_i. The centre to centre distance is H and the angular velocities ω_i are again prescribed, which is simpler than specification of corresponding transmitted moments. Contrary to the finite element model, we place the Cartesian coordinate frame $[\boldsymbol{i}, \boldsymbol{j}]$ in the centre of the corresponding, left pulley.

For completeness we need to remark that some minor provisions have

to be made to guarantee that the here deduced equations hold for the second belt segment as well. Firstly, a different Cartesian basis needs to be introduced, which sits in the centre of the opposite, right pulley with the horizontal unit vector pointing from right to left and the vertical unit vector pointing downwards, such that if we rotated the drive about 180° the situation for the second segment would look just like the one shown in Figure 2, the only difference being that the gravity G then acts in the opposite direction. Therefore, we would have to change the sign of every instance of G in the upcoming formulas. Lastly, we would have to switch the indices of pulley parameters $\{R_1, \omega_1\} \leftrightarrow \{R_2, \omega_2\}$.

After these preliminaries, let us focus solely on the first belt segment for the rest of this section. As Figure 2 suggests, two spatial coordinates, the angle φ and the position x in direction $\boldsymbol{i}$, are used to parametrise the position vector $\boldsymbol{r}$ in any one of the three solution regions. Specifically, the coordinate x is used for parametrisation in the free span region, whereas the angle φ applies to the sticking and the sliding region. The tangential unit vector $\boldsymbol{t}$ and the outward-pointing unit vector $\boldsymbol{n}$ are also written as functions of φ

$$\boldsymbol{t} = -\boldsymbol{i}\sin(\varphi) + \boldsymbol{j}\cos(\varphi)\ , \qquad \boldsymbol{t}' = -\boldsymbol{n}\,\varphi' \tag{29a}$$

$$\boldsymbol{n} = \boldsymbol{i}\cos(\varphi) + \boldsymbol{j}\sin(\varphi)\ , \qquad \boldsymbol{n}' = \boldsymbol{t}\,\varphi'\,. \tag{29b}$$

In contrast to the mixed finite element description with one circumferential coordinate σ, compare Figure 1, the sizes of the polar and Cartesian coordinate domains are no longer fixed, but depend on the actual positions of the touching points A, C and D. The second point B marks the transition from the sticking to the sliding region. We introduce corresponding angles ψ_A to ψ_D, which are measured against the horizontal direction $\boldsymbol{i}$ just like φ, to mathematically describe these positions. For the sub-problem of the first belt segment at hand only the three constants ψ_B, ψ_C and ψ_D are regarded unknown, but ψ_A formally belongs to the adjacent segment and is

thus considered to be a given parameter. This is due to the fact that the touching point A of the belt segment under consideration coincides with the run-up point D of the second segment and vice versa. Thus, if we use Roman numerals to index the individual segments, we can formulate constraints at each transition point of the two segments

$$\psi_{\mathrm{A}}^{\mathrm{I}} = \psi_{\mathrm{D}}^{\mathrm{II}} - \pi\,, \quad \psi_{\mathrm{A}}^{\mathrm{II}} = \psi_{\mathrm{D}}^{\mathrm{I}} - \pi\,, \tag{30}$$

where a constant offset by π is introduced due to Cartesian system of the segment II being rotated by 180°. We will later discover that the angle ψ_{A} is merely needed to set the origin of the segment-wise material coordinate s. The actual value of ψ_{A} is thus insignificant for the solution in a single segment, but important when it comes to the formulation of the closing condition in Subsection 3.4.

The governing equations of the underlying planar theory of extensible strings in Lagrangian form read [5]

$$\partial_s\,(Q\,\boldsymbol{t}) + \boldsymbol{q} = \rho\,\boldsymbol{w} \tag{31a}$$

$$\hat{Q} = b\,\epsilon \tag{31b}$$

$$\epsilon = \frac{1}{2}\,\left(\Gamma^2 - 1\right) \tag{31c}$$

$$\text{with} \quad Q = \Gamma\,\hat{Q}\,, \quad \Gamma = |\partial_s \boldsymbol{r}|\,. \tag{31d}$$

The balance of linear momentum (31a) connects the axial force Q (no transverse forces in a string model) and the distributed forces $\boldsymbol{q}$ to the inertia terms on the right side, with ρ being the mass per material length and $\boldsymbol{w}$ denoting the acceleration. For comparison purposes, we again use the Green strain measure ϵ, which is directly connected to the stretch Γ and proportional to its conjugate force $\hat{Q}$ with the tensile stiffness b. This new force quantity is related to the actual axial force that appears in the balance equation by $Q = \Gamma\,\hat{Q}$, see [25] for a brief comparison and [8] for an in-depth discussion

on the topic of strain measures in beam theory.

We will in the following address each solution region (stick, slip, free span) of the depicted belt segment separately and finally formulate the closing condition to conclude the system of equations for the belt drive as a whole. In an effort to write equations more concisely, we will use Γ extensively in the upcoming expressions, but regard $\hat{Q}$ as a major unknown. Both are directly related through the constitutive equation (31b) and the thereby deduced replacement rules read

$$\Gamma = \sqrt{1 + 2\,\frac{\hat{Q}}{b}}\,, \quad \Gamma' = \frac{\hat{Q}'}{b\,\Gamma}\,. \tag{32}$$

3.1. Sticking friction region

Provision of the constant material transport rate $\partial_t s = c$ allows full determination of the solution in the sticking region. When assuming full contact between belt and pulley, the position vector and its material derivative, with the help of (29b), follow to

$$\boldsymbol{r} = R_1\,\boldsymbol{n}\,, \quad \partial_s \boldsymbol{r} = R_1\,\partial_s\varphi\,\boldsymbol{t}\,. \tag{33}$$

Next, we write the material coordinate as $s = s\,(\varphi,\, t)$, compute its first derivatives

$$\partial_s s = 1 = \partial_\varphi s\,\partial_s\varphi \tag{34a}$$

$$\mathring{\partial}_t s = 0 = \partial_\varphi s\,\mathring{\partial}_t\varphi + c\,, \tag{34b}$$

and make immediate use of (34a) to substitute $\partial_s\varphi$ in (33) when computing the stretch

$$\Gamma = |\partial_s \boldsymbol{r}| = R_1\ (\partial_\varphi s)^{-1}\ . \tag{35}$$

The pure sticking contact in the considered region forces the belt to move together with the pulley surface. Therefore, the corresponding material points

Journal Pre-proofs

Journal Pre-proofs

travel with the same angular velocity, which translates to $\mathring{\partial}_t \varphi = \omega_1$. Using this relation we evaluate (34b) further taking (35) into account and conclude that the stretch in the sticking region is constant,

$$\Gamma = -\frac{R_1\,\omega_1}{c} = \text{const}\,. \tag{36}$$

Moreover, this expression effectively sets a range for plausible values of c, because the belt must not move backwards and fulfilment of $\Gamma \geq 1$ to keep the belt under tension requires $c \in [-R_1\,\omega_1,\,0]$. As a consequence, the axial force, according to (31b), is constant as well,

$$\hat{Q} = \frac{b}{2}\,\left(\Gamma^2 - 1\right) = \text{const}\,. \tag{37}$$

To compute the material arc coordinate s we rearrange and integrate (35), choosing the time dependent integration constant such that the expression fits the steady state form (16)

$$s = \frac{R_1}{\Gamma}\,(\varphi - \psi_\text{A}) + c\,t\,. \tag{38}$$

To allocate the position of $s = 0$ we simply set $s\,(\psi_\text{A}, 0) = 0$, indicating that the segment's material length s originates at ψ_A.

For the sake of completeness we further evaluate the balance equation (31a) to deduce the contact forces. The acceleration reduces to the centripetal part $\boldsymbol{w} = -R_1\,\omega_1^2\,\boldsymbol{n}$ since material elements cannot be accelerated in tangential direction when sticking. The gravitational force G acts in opposite direction of $\boldsymbol{j}$ in the current setting, and the contact forces consist of the tangential traction $\tau_\perp$ and the normal contact pressure $\tau_\text{N} \geq 0$, such that the distributed load can be written as

$$\boldsymbol{q} = (\tau_\perp - G\cos(\varphi))\;\boldsymbol{t} + (\tau_\text{N} - G\sin(\varphi))\;\boldsymbol{n}\,. \tag{39}$$

With $\partial_s \varphi = \Gamma / R_1$ to substitute in (29a) the material derivative of the axial force reads

$$\partial_s \left(Q\, \boldsymbol{t} \right) = \Gamma\, \hat{Q}\, \partial_s \boldsymbol{t} = - \left(\frac{\Gamma^2}{R_1}\, \hat{Q} \right) \boldsymbol{n} \,. \tag{40}$$

Finally, we obtain the contact forces after evaluation of the balance equation and projection onto the tangential and normal direction

$$\tau_\perp = G \cos(\varphi) \;, \quad \tau_\mathrm{N} = \frac{\Gamma^2}{R_1}\, \hat{Q} - \rho\, R_1\, \omega_1^2 + G \sin(\varphi) \;. \tag{41}$$

3.2. Sliding friction region

The sliding friction portion of the contact zone is again parametrised with φ. Hence, formulas (33) still hold in this region and the definition of the stretch (35) now serves as a differential equation for the material coordinate s

$$\partial_\varphi s = \frac{R_1}{\Gamma} \,, \tag{42}$$

which further defines the transformation of material derivatives

$$\partial_s = \partial_s \varphi\, \partial_\varphi = \left(\partial_\varphi s \right)^{-1} \partial_\varphi = \frac{\Gamma}{R_1}\, \partial_\varphi \,. \tag{43}$$

However, as a material particle may now travel at a different speed than the corresponding point on the pulley (34b) can only be rearranged for later substitution

$$\mathring{\partial}_t \varphi = - \frac{\Gamma}{R_1}\, c \,. \tag{44}$$

The distributed forces can still be written in the form of (39) and after some derivations we obtain the material derivative of the axial force

$$\partial_s \left(Q\, \boldsymbol{t} \right) = \partial_\varphi \hat{Q}\, \frac{3\,\Gamma^2 - 1}{2\, R_1}\, \boldsymbol{t} - \frac{\hat{Q}\, \Gamma^2}{R_1}\, \boldsymbol{n} \,. \tag{45}$$

Journal Pre-proofs

We differentiate the position vector $\boldsymbol{r}$ twice with respect to time to compute the acceleration

$$\boldsymbol{w} = \mathring{\partial}_t \left(\mathring{\partial}_t \boldsymbol{r} \right) = \mathring{\partial}_t \left(-\Gamma \, c \, \boldsymbol{t} \right) = \frac{\partial_\varphi \hat{Q} \, c^2}{b \, R_1} \, \boldsymbol{t} + \frac{\left(\Gamma \, c \right)^2}{R_1} \, \boldsymbol{n} \, . \tag{46}$$

One has to make use of the constitutive relations (31b) and (32), substitute the derivatives of unit vectors according to (29) with $\partial_s \varphi = \Gamma / R_1$ and replace $\mathring{\partial}_t \varphi$ with (44) to arrive at the above formulas (45) and (46) in their presented form. After insertion into the balance equation and projection onto $\boldsymbol{n}$, we derive the contact forces with the help of the Coulomb friction criterion

$$\tau_{\mathrm{N}} = \frac{\Gamma^2}{R_1} \left(\hat{Q} - \rho \, c^2 \right) + G \sin(\varphi) \tag{47a}$$

$$\tau_\perp = \mu \, \tau_{\mathrm{N}} \, . \tag{47b}$$

Here the friction coefficient μ is to be interpreted as a signed quantity. The sign depends on the direction of sliding motion. In case of forward sliding motion it is negative and otherwise positive. One can either prescribe the direction of sliding motion assuming backward sliding on driving and forward sliding on driven pulleys or determine it by comparison of belt and pulley velocities

$$\operatorname{sign}(\mu) = \operatorname{sign} \left(\omega_1 - \mathring{\partial}_t \varphi \right) \, . \tag{48}$$

Substitution of $\tau_\perp$ in the balance equation and projection onto $\boldsymbol{t}$ yields the sought for differential equation for $\hat{Q}$

$$\partial_\varphi \hat{Q} \left(\frac{3 \, \Gamma^2 - 1}{2 \, R_1} - \frac{\rho \, c^2}{b \, R_1} \right) + \tau_\perp - G \cos(\varphi) = 0 \, . \tag{49}$$

If c and estimates for the angles ψ_{A} and ψ_{B} are provided, we can compute the solution in a single sliding region by integration of an initial value problem with the ODEs (49) and (42) for the axial force $\hat{Q}$ and the coordinate s, respectively. The corresponding initial conditions just demand continuity of

Journal Pre-proofs

$\{\hat{Q},\, s\}$ at the transition point $\varphi = \psi_{\mathrm{B}}$ between sticking and slipping region.

3.3. Free span region

In accordance with Figure 2, we write the position vector of particles and its first material derivative in the free span region as

$$\boldsymbol{r} = x\,\boldsymbol{i} + y\,(x,\,t)\;\boldsymbol{j}\,, \quad \partial_s \boldsymbol{r} = \partial_s x\,\boldsymbol{i} + \partial_s y\,\boldsymbol{j}\,. \tag{50}$$

In full analogy to (34a) we derive an equivalent transformation rule for the Cartesian parametrisation of the material coordinate $s = s\,(x,\,t)$

$$\partial_s x = (\partial_x s)^{-1}\,. \tag{51}$$

With this in mind, we can rewrite the material derivative of the position vector as $\partial_s \boldsymbol{r} = \Gamma\,\boldsymbol{t}$ and compare its Cartesian components with (50)

$$\partial_x s = \frac{-1}{\Gamma\sin(\varphi)}\,, \quad \partial_x y = -\cot(\varphi)\;. \tag{52}$$

Consequently, the transformation of material derivatives becomes

$$\partial_s = (-\Gamma\sin(\varphi))\;\partial_x\,. \tag{53}$$

The vector of distributed forces now lacks the contact forces and we deduce the remaining components of the balance equation in a similar fashion

$$\boldsymbol{q} = -G\cos(\varphi)\;\boldsymbol{t} - G\sin(\varphi)\;\boldsymbol{n} \tag{54a}$$

$$\partial_s\,(Q\,\boldsymbol{t}) = \left(-\partial_x\hat{Q}\sin(\varphi)\;\frac{3\,\Gamma^2-1}{2}\right)\boldsymbol{t} + \Big(\partial_x\varphi\,\hat{Q}\,\Gamma^2\sin(\varphi)\Big)\;\boldsymbol{n} \tag{54b}$$

$$\boldsymbol{w} = \left(-\partial_x\hat{Q}\,\frac{c^2\sin(\varphi)}{b}\right)\boldsymbol{t} + \big(\partial_x\varphi\,c^2\,\Gamma^2\sin(\varphi)\big)\;\boldsymbol{n}\,. \tag{54c}$$

Journal Pre-proofs

After insertion in the balance equation, evaluation of tangential and normal components and some rearrangements we obtain

$$\partial_x \varphi \left(\hat{Q}\,\Gamma^2 - \rho\, c^2\,\Gamma^2 \right) = G \tag{55a}$$

$$\partial_x \hat{Q} \left(-\frac{3\,\Gamma^2 - 1}{2} + \frac{\rho\, c^2}{b} \right) = G \cot(\varphi) \ , \tag{55b}$$

which concludes the system of ODEs (52) and (55) for $\{s,\, y,\, \varphi,\, \hat{Q}\}$. Noticeably, the angle φ, previously used for parametrisation in the contact domain, is considered a major unknown in the free span region.

To integrate the corresponding boundary value problem in the free span region for a given transport rate c, we need to define seven conditions to determine the four integration constants for the system of ODEs as well as the unknown angles $\{\psi_\mathrm{B},\, \psi_\mathrm{C},\, \psi_\mathrm{D}\}$. In this respect, we simply demand continuity for $\{s,\, y,\, \varphi,\, \hat{Q}\}$ at the run-off point C and for $\{y,\, \varphi,\, \hat{Q}\}$ at the run-up point D, which marks the transition to the sticking zone on the opposite pulley. Since the matching conditions at C depend on the solution in the sliding region, the initial value problem for the sliding part needs to be solved each time the boundary conditions for the free span require evaluation. On the other hand, calculation of the right side conditions at D is a simple task, because the solutions in the sticking regions are known in advance for a given value of c.

3.4. Iterative solution of the boundary value problem

To obtain the solution for a single belt segment, we rely on the standard purpose solvers ode45 and bvp4c as implemented in the software Matlab for the numerical integration of the initial and boundary value problems. To make the problem with unknown boundaries accessible to the collocation solver, we first need to transform it to a system with fixed boundaries in a normalised coordinate $\xi \in [0,\, 1]$. This well known strategy involves coordinate conversions of the form $\varphi = \varphi(\xi)$ and $x = x(\xi)$ that are quite similar to

Journal Pre-proofs

Journal Pre-proofs

the ones introduced for s and we refer to [2, 10] for applications of the same technique.

To construct an appropriate initial guess for the unknown fields and constants we replicate the deflection-less configuration of the belt that resembles the classic case of a tight belt ($\lambda < 1$) without gravity. To specify this initial guess, let us assume equal pulleys ($R_1 = R_2 = R$) for simplicity; the required adaptions for $R_1 \neq R_2$ are straightforward. In this special case the transition point angles are approximated as $\psi_\mathrm{A} = \pi/2$, $\psi_\mathrm{B} = \pi$ and $\psi_\mathrm{C} = \psi_\mathrm{D} = 3\,\pi/2$, where ψ_B is assumed to split the contact zone in half. The vertical deflection $y = -R$ and the angle $\varphi = 3\,\pi/2$ are constant, whereas the material coordinate s and the force $\hat{Q}$ are interpolated linearly between their two values at C and D

$$s\,(\xi) = s|_\mathrm{C} + H\,\xi\,, \quad \hat{Q}\,(\xi) = \hat{Q}\Big|_\mathrm{C} + \left(\hat{Q}\Big|_\mathrm{D} - \hat{Q}\Big|_\mathrm{C}\right)\,\xi\,. \tag{56}$$

As outlined before, the values at C are obtained through integration of the initial value problem in the sliding region. The interpolation for the material coordinate s ignores the stretching of the string. Evidently, seeking a steady-state solution starting from this basic initial configuration might fail in cases with very large transverse deflections ($\lambda > 1$). Then an iterative approach is in order with the length-ratio λ serving as homotopy parameter. Finally, equation (36) evaluated for $\Gamma \approx 1/\lambda$ provides a solid initial guess for c.

To complete the solution procedure for the whole belt drive, it remains to formulate the closing condition as a root problem for the appropriate material transport rate c: The material coordinate s of a single belt segment is strictly growing from the start A to the end D. For the stationary state the same amount of material is contained between these interval borders at any time such that the segment's material length can be computed as the difference of material coordinates at these two points. The total length of the belt is a sum of the lengths of its individual segments, which is used to formulate the

geometry	$R_1 = R_2 = 0.15$	$H = 2$	$\lambda = 1.0$
material	$b = 12.5$	$\rho = 0.03$	
pulleys	$\mu = 0.4$	$\omega_1 = 10$	$\omega_2 = 9.8$

Table 2: SI values of the benchmark problem; the gravity constant is $g = 9.81$

closing condition

$$s_{\max} = \sum_{i=\mathrm{I},\,\mathrm{II}} \left(s|_{\mathrm{D}} - s|_{\mathrm{A}} \right)^i , \tag{57}$$

where Roman numerals are used once again to denote the individual segments. Since $s|_{\mathrm{A}}$ equals (38) for $\varphi = \psi_{\mathrm{A}}$ the above equation can be further simplified to

$$s_{\max} = \sum_{i=\mathrm{I},\,\mathrm{II}} \left(s|_{\mathrm{D}} - c\,t \right)^i , \tag{58}$$

which demonstrates mass continuity in the considered control volume, because, for the above relation to hold at all times, the same amount of material entering at point A of a segment must exit at D. The constraint (58) is referred to as "compatibility condition" in [18] and ensures that the found solution indeed corresponds to a belt with the specified length $s_{\max}$ in the undeformed state. Hence, the adopted strategy resembles a shooting method trying to find the appropriate value of c such that the above condition is met. A simple secant method is used to iteratively solve this root problem.

4. Results and comparison

We consider the model parameters given in Table 2, which correspond to a slackly mounted extensible string moving at moderate speed. All quantities are presented in the SI system of units. The gravitational constant is assumed to be $g = 9.81$ and the pulleys rotate in counter-clockwise direction. The angular velocities are high enough that stationary inertia effects are visible, but far from being dominant.

Journal Pre-proofs

Figure 3 presents two deformed configurations of the belt obtained with the FES_0 type of analysis, i.e. stationary inertia effects are neglected. The used mesh is refined in the contact regions and has a total number of 1090 elements. This discretisation level is too fine to plot, but the distribution of nodal points along the contour coordinate σ is simply more dense than the one presented in Figure 1. The depicted state for $t = 0$ corresponds to the initial, frictionless static equilibrium and $t \to \infty$ indicates the steady state as a final result of the intermediate transition process. During this transient phase sliding friction regions evolve originating from the run-off points, where the belt loses contact with a pulley and enters the successive free-span region. Moreover, material is continuously rearranged from the upper span to the lower span leading to a tightening of the former and relaxation of the latter.

We forgo printing an analogous graphic for the simulation with inclusion of inertia effects (FES_T), because the differences are very subtle and the two graphics would be almost indistinguishable. Instead we present some numeric data in the two Tables 3 and 4 corresponding to the FES_0 and the FES_T analysis, respectively. Each Table displays some characteristic values of the steady state obtained with both the finite element scheme as well as by numeric integration of the boundary value problem (BVP). The relative error measures show the reached accuracy of the finite element simulations in comparison to the quasi-converged results of the semi-analytic solutions. Both the transverse deflections ν and the axial strains ϵ are evaluated at the middle point of the lower span, as indicated in Figure 3. In contrast to the first three columns in the Tables, which are given in SI units, the sticking region and the sliding region size, $\Delta\psi_{\mathrm{stick}}$ and $\Delta\psi_{\mathrm{slip}}$, are presented in degrees for convenience. The driving moment M can be computed as a line integral over distributed moments, which are attributed to the tangential tractions

$$M_{\mathrm{FES}} = -\sum_{\mathrm{el}} \int_{-1}^{1} \tau_{\perp}\, R\, \partial_{\sigma} s\, \partial_{\xi} \sigma \, \mathrm{d}\xi \,, \quad M_{\mathrm{BVP}} = \int_{\psi_{\mathrm{A}}}^{\psi_{\mathrm{C}}} \tau_{\perp}\, R\, \partial_{\varphi} s \, \mathrm{d}\varphi \,. \tag{59}$$

For the finite element version we obviously have to restrict the sum to elements in contact with the driving pulley in order to avoid contributions from the opposite, driven side. The corresponding element integrals are again transformed to Gaussian quadratures and the stored Lagrangian multiplier estimates are used to evaluate $\tau_\perp$ at each integration point. The sign change in front again stems from the fact that the finite element tangential tractions point in opposite direction of the physical ones.

Overall, the finite element results correspond well to the practically converged, numerical integration of the boundary value problem. The contact region angles, $\Delta\psi_{\text{stick}}$ and $\Delta\psi_{\text{slip}}$, are the least accurate quantities, because the accuracy of contact resolution is limited by the distance of adjacent integration points. Improved results may be obtained with further refinement of the contact domain at expense of computation time. As one would expect, inclusion of stationary inertia effects induces higher strains, increases driving torque as well as transverse deflections in the slack span and decreases the contact domain size.

Figure 4 presents some additional results for the specified parameter set, inertia effects being neglected (FES_0). The steady state distribution of axial strains is shown in the left diagram. The vertical bars encapsulate the contact regions on both pulleys. As predicted by the analytic considerations, ϵ remains constant in the sticking regions and, in obvious resemblance with classic creep-theory solutions, the strain transition in the sliding regions (from tight to slack for the driving side or vice versa for the driven side) is essentially linear. The strain variation in the free span region is entirely attributed to the influence of the gravitational force. The graph on the right side of Figure 4 demonstrates mesh convergence of the proposed finite element scheme on the example of the axial strain evaluated at the middle of the lower span. Convergence is fast reaching accurate results with slightly over 100 elements, but not monotonous. In fact, the absolute value of the error measure had to be taken, because finite element evaluations for different

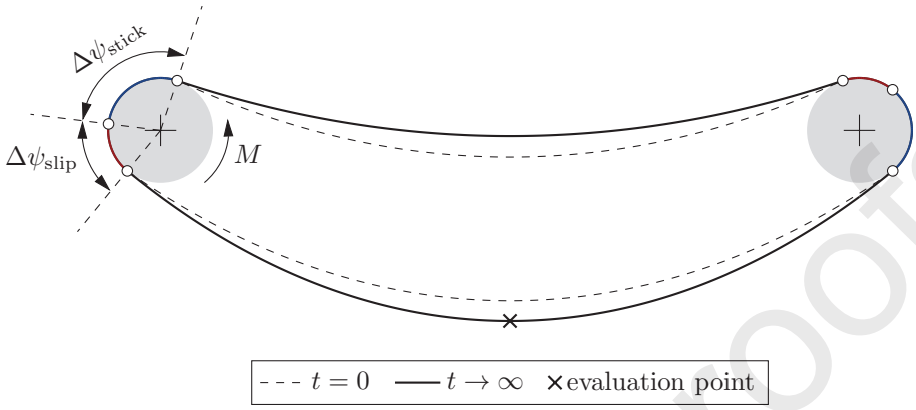

Figure 3: Initial and final steady state configurations of the belt drive as obtained with the FES_0 analysis

	ν	ϵ	M	$\Delta\psi_{\text{stick}}$	$\Delta\psi_{\text{slip}}$
BVP_0	0.395 39	0.032 31	0.035 30	101.1610°	58.0764°
FES_0	0.395 36	0.032 31	0.035 30	101.7040°	57.4195°
$1 - \frac{x_{\text{FES}}}{x_{\text{BVP}}}$	7.722 e−5	−6.069 e−5	3.321 e−5	−5.369 e−3	1.131 e−2

Table 3: Comparing finite element results to reference values obtained through numeric integration of the steady state boundary value problem; parameters taken from Table 2; stationary inertia effects are ignored (FES_0)

	ν	ϵ	M	$\Delta\psi_{\text{stick}}$	$\Delta\psi_{\text{slip}}$
BVP_T	0.413 23	0.035 69	0.035 86	98.7960°	59.2447°
FES_T	0.413 27	0.035 69	0.035 91	99.4665°	58.5714°
$1 - \frac{x_{\text{FES}}}{x_{\text{BVP}}}$	−1.052 e−4	7.636 e−5	−1.442 e−3	−6.787 e−3	1.136 e−2

Table 4: Comparing finite element results to reference values obtained through numeric integration of the steady state boundary value problem; parameters taken from Table 2; taking stationary inertia effects into account (FES_T)

Journal Pre-proofs

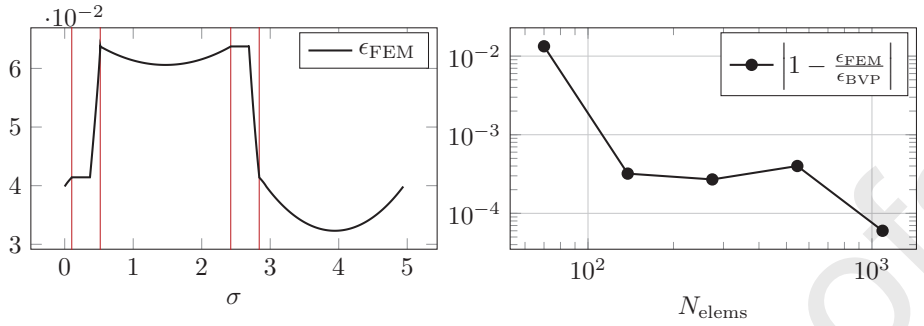

Figure 4: Steady state distribution of axial strains over σ (left) and finite element mesh convergence of ϵ at the middle of the lower span compared to the semi-analytic results (right); no account for inertia effects (FES_0)

discretisation levels oscillate around the converged semi-analytic result gradually decreasing the amplitude with increasing number of elements. It comes as no surprise that convergence is not monotonous for the steady state, since even the frictionless static solution shows the same behaviour [26]. Aside from the total number of finite elements used, the chosen placement of nodal points determines the reachable accuracy of a particular model. Hence, performance could probably be increased further through improved placement of nodal points. The ability to use refined meshes for axially moving structures without ever having to remesh the model is an important advantage of the mixed E.L.-type of elements over conventional ones. The latter are practically condemned to use equally spaced, fine meshes throughout the whole model in order to ensure sufficient resolution of the contact domain when material nodes travel in axial direction.

Figure 5 is devoted to the time evolution of the contact region at the driving pulley, which was simulated with the FES_0 type of analysis. The left graphic displays the development of the axial strains ϵ at the two touching points that encapsulate the contact domain. The dashed curve corresponds to the point of first contact, where the belt adheres to the pulley surface approaching it from the upper, tight span. The solid line relates to the point of contact loss, from where the belt enters the lower, slack span region. In

Journal Pre-proofs

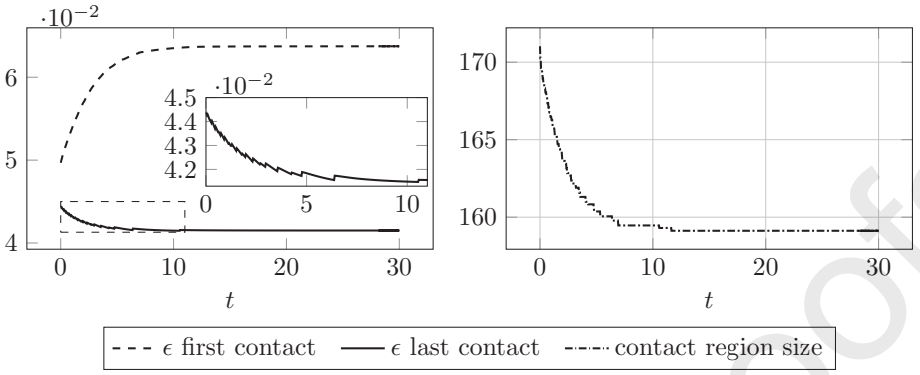

Figure 5: Time evolution of strains at touching points and contact region size in degrees at the left driving pulley; no account for inertia effects (FES_0)

the course of time simulation these bordering points move slowly along the pulley contour, gradually decreasing the total size of the contact domain, which is depicted in the right picture given in degrees. Naturally, strains in the point adjacent to the tight span region increase with respect to time and the opposite holds true for the point preceding the slack span region.

The magnified detail picture on the left demonstrates that the graph is in fact not smooth, but shows a zig-zag like behaviour with decreasing frequency. The same holds true for the development of the contact region size in the right diagram. These effects are again a consequence of the discrete resolution of contact states at element integration points. Due to their finite distance the shrinking of the contact zone can only be resolved discretely. The corresponding peaks in the evolution of strains occur due to a change in the load distribution as a consequence of single integration points loosing contact instantaneously. The frequency of such oscillations is high in the early stages of the simulation but decreases continuously as the belt slowly approaches its stationary contour motion. A higher degree of smoothness could again be achieved by further refining finite element meshes in the prospective contact zones, which would minimize integration point distances. Nevertheless, the depicted graphs are quite smooth already and free of other

Journal Pre-proofs

spurious oscillations, which typically arise in conventional finite element simulations [15].

5. Conclusion

The planar, static, E.L.-finite element model, previously introduced in [26], has been successfully extended to simulate the quasistatic, transient motion of a simple two-pulley belt drive. Gravity is taken into account and stationary inertia effects may be considered as well. The simulation starts from a previously acquired, frictionless equilibrium position and the following transient phase finally leads into stationary contour motion, characterised by a fixed spatial configuration through which material particles keep travelling at constant mass transport rate. During this process the pulleys rotate with constant speeds ω_i and transfer their rotary motion to the belt by means of Coulomb dry friction contact.

A major part of the present contribution is devoted to the appropriate implementation of frictional contact in the existing finite element framework. In this regard, a variant of the augmented Lagrangian treatment is proposed. This strategy is based on the simple penalty method, which is extended with an iterative update of stored Lagrange multiplier estimates for normal and tangential contact tractions. Presently, the finite element simulations are limited to the simpler model of an extensible string, as the inclusion of bending effects proves a difficult task due to concentrated contact interactions at the touching points that inhibit the augmented Lagrangian contact treatment [26].

The mixed kinematic approach features finite element parametrisation in a compound, spatial coordinate σ, which consists of polar and Cartesian domains. In this description, nodal points may only travel in transverse direction, while material is transported through the mesh in axial direction. It is advantageous compared to classic Lagrangian type finite elements due to:

- contact resolution at fixed integration points in space, which promotes convergence of contact state data,
- the ability to use refined meshes in the contact zones or particular regions of interest,
- suppression of spurious oscillations by prohibiting the motion of nodal points in axial direction,
- easy identification of steady states by time independence of nodal deflection variables.

In addition, the steady state solution is reproduced semi-analytically by numeric integration of the corresponding boundary value problem. The examined analytic problem of an extensible string enqueues in a series of similar models available in the literature. Its account for the influence of gravity is a novel feature with particular importance for the considered problem of a slackly spanned belt. Optionally, stationary inertia effects can be included as well, which are negligible at low speeds but recognisable for the medium velocity case studied.

Considering a particular benchmark example, the obtained finite element results for the stationary state correspond well to the semi-analytic reference computations. The steady state strain distribution in the contact region bears close resemblance with classic belt-creep theory and strain variations in the free span regions relate to the account for gravity. Investigating time evolution of strains at the bordering points of a contact region, we obtain essentially smooth curves with minor oscillatory discontinuities. The latter are a consequence of the discrete contact resolution at individual integration points in conjunction with the continuous movement of the contact zone border during transient motion and are thus inherent to the proposed finite element scheme.

In conclusion, the present contribution clearly demonstrates the capability of the proposed finite element framework to simulate quasistatic belt

Journal Pre-proofs

drive motion, but it also leaves some potential research topics for the future, such as:

- the extension of the analytic model to a true beam with non-zero bending stiffness,
- the improvement of the contact model to allow for augmented Lagrangian treatment for problems with bending stiffness,
- a method to directly obtain steady state solutions in the finite element framework without the need to run through the whole transient process.

Acknowledgement

Support by the Austrian Research Promotion Agency (FFG), project number 861493, is gratefully acknowledged.

Journal Pre-proofs

References

[1] Bechtel, S. E., Vohra, S., Jacob, K. I., Carlson, C. D., 09 1999. The Stretching and Slipping of Belts and Fibers on Pulleys. Journal of Applied Mechanics 67 (1), 197–206.
URL https://doi.org/10.1115/1.321164

[2] Belyaev, A. K., Eliseev, V. V., Irschik, H., Oborin, E. A., Dec 2017. Contact of two equal rigid pulleys with a belt modelled as cosserat nonlinear elastic rod. Acta Mechanica 228 (12), 4425–4434.
URL https://doi.org/10.1007/s00707-017-1942-0

[3] Belyaev, A. K., Eliseev, V. V., Irschik, H., Oborin, E. A., jun 2018. Static contact of belt and pulleys with account for shear and gravity. Journal of Physics: Conference Series 1048, 012002.
URL https://doi.org/10.1088%2F1742-6596%2F1048%2F1%2F012002

[4] Dufva, K., Kerkkänen, K., Maqueda, L. G., Shabana, A. A., Jun 2007. Nonlinear dynamics of three-dimensional belt drives using the finite-element method. Nonlinear Dynamics 48 (4), 449–466.
URL https://doi.org/10.1007/s11071-006-9098-9

[5] Eliseev, V., Vetyukov, Y., Aug 2012. Effects of deformation in the dynamics of belt drive. Acta Mechanica 223 (8), 1657–1667.
URL https://doi.org/10.1007/s00707-012-0675-3

[6] Ghayesh, M. H., Kafiabad, H. A., Reid, T., 2012. Sub- and super-critical nonlinear dynamics of a harmonically excited axially moving beam. International Journal of Solids and Structures 49 (1), 227 – 243.
URL http://www.sciencedirect.com/science/article/pii/S0020768311003374

Journal Pre-proofs

[7] Hoffman, J., Jansson, J., Stöckli, M., 2011. Unified continuum modeling of fluid-structure interaction. Mathematical Models and Methods in Applied Sciences 21 (03), 491–513.
URL https://doi.org/10.1142/S021820251100512X

[8] Irschik, H., Gerstmayr, J., Jul 2009. A continuum mechanics based derivation of Reissner's large-displacement finite-strain beam theory: the case of plane deformations of originally straight Bernoulli–Euler beams. Acta Mechanica 206 (1), 1–21.
URL https://doi.org/10.1007/s00707-008-0085-8

[9] Kim, D., Leamy, M., Ferri, A., 08 2009. Dynamic Modeling of Flat Belt Drives Using the Elastic-Perfectly-Plastic Friction Law. In: Proceedings of the ASME Design Engineering Technical Conference. Vol. Volume 4: 7th International Conference on Multibody Systems, Nonlinear Dynamics, and Control, Parts A, B and C of International Design Engineering Technical Conferences and Computers and Information in Engineering Conference. pp. 483–491.
URL https://doi.org/10.1115/DETC2009-87296

[10] Kong, L., Parker, R. G., 02 2005. Steady Mechanics of Belt-Pulley Systems. Journal of Applied Mechanics 72 (1), 25–34.
URL https://doi.org/10.1115/1.1827251

[11] Leamy, M. J., 10 2004. On a Perturbation Method for the Analysis of Unsteady Belt-Drive Operation. Journal of Applied Mechanics 72 (4), 570–580.
URL https://doi.org/10.1115/1.1940660

[12] Leamy, M. J., Wasfy, T. M., 12 2002. Transient and Steady-State Dynamic Finite Element Modeling of Belt-Drives. Journal of Dynamic Systems, Measurement, and Control 124 (4), 575–581.
URL https://doi.org/10.1115/1.1513793

Journal Pre-proofs

[13] Mojdehi, A. R., Holmes, D. P., Dillard, D. A., 2017. Friction of extensible strips: An extended shear lag model with experimental evaluation. International Journal of Solids and Structures 124, 125 – 134.
URL http://www.sciencedirect.com/science/article/pii/S0020768317302858

[14] Nordenholz, T. R., O'Reilly, O. M., 09 1995. On Kinematical Conditions for Steady Motions of Strings and Rods. Journal of Applied Mechanics 62 (3), 820–822.
URL https://doi.org/10.1115/1.2897023

[15] Oborin, E., Vetyukov, Y., Steinbrecher, I., 2018. Eulerian description of non-stationary motion of an idealized belt-pulley system with dry friction. International Journal of Solids and Structures 147, 40 – 51.
URL http://www.sciencedirect.com/science/article/pii/S0020768318301513

[16] Pechstein, A., Gerstmayr, J., Oct 2013. A Lagrange–Eulerian formulation of an axially moving beam based on the absolute nodal coordinate formulation. Multibody System Dynamics 30 (3), 343–358.
URL https://doi.org/10.1007/s11044-013-9350-2

[17] Radi, B., Baba, O., Gelin, J.-C., 1998. Treatment of the frictional contact via a Lagrangian formulation. Mathematical and Computer Modelling 28 (4), 407 – 412.
URL http://www.sciencedirect.com/science/article/pii/S0895717798001307

[18] Rubin, M. B., 05 2000. An Exact Solution for Steady Motion of an Extensible Belt in Multipulley Belt Drive Systems. Journal of Mechanical Design 122 (3), 311–316.
URL https://doi.org/10.1115/1.1288404

Journal Pre-proofs

[19] Simo, J., Laursen, T., 1992. An augmented Lagrangian treatment of contact problems involving friction. Computers & Structures 42 (1), 97 – 116.
URL http://www.sciencedirect.com/science/article/pii/0045794992905406

[20] Steinbrecher, I., Humer, A., Vu-Quoc, L., 2017. On the numerical modeling of sliding beams: A comparison of different approaches. Journal of Sound and Vibration 408, 270 – 290.
URL http://www.sciencedirect.com/science/article/pii/S0022460X17305357

[21] Synka, J., Kainz, A., 2003. A novel mixed Eulerian-–Lagrangian finite-element method for steady-state hot rolling processes. International Journal of Mechanical Sciences 45 (12), 2043 – 2060.
URL http://www.sciencedirect.com/science/article/pii/S0020740303002388

[22] Ulsoy, A., Mote, C., 02 1982. Vibration of wide band saw blades. ASME Journal of Engineering for Industry 104, 71–78.

[23] Vetyukov, Y., 2018. Non-material finite element modelling of large vibrations of axially moving strings and beams. Journal of Sound and Vibration 414, 299 – 317.
URL http://www.sciencedirect.com/science/article/pii/S0022460X17307824

[24] Vetyukov, Y., Gruber, P. G., Krommer, M., Gerstmayr, J., Gafur, I., Winter, G., 2017. Mixed Eulerian–-Lagrangian description in materials processing: deformation of a metal sheet in a rolling mill. International Journal for Numerical Methods in Engineering 109 (10), 1371–1390.
URL https://onlinelibrary.wiley.com/doi/abs/10.1002/nme.5314

Journal Pre-proofs

[25] Vetyukov, Y., Oborin, E., Krommer, M., Eliseev, V., 2017. Transient modelling of flexible belt drive dynamics using the equations of a deformable string with discontinuities. Mathematical and Computer Modelling of Dynamical Systems 23 (1), 40–54.
URL https://doi.org/10.1080/13873954.2016.1232281

[26] Vetyukov, Y., Oborin, E., Scheidl, J., Krommer, M., Schmidrathner, C., 2019. Flexible belt hanging on two pulleys: Contact problem at non-material kinematic description. International Journal of Solids and Structures 168, 183 – 193.
URL http://www.sciencedirect.com/science/article/pii/S0020768319301581

[27] Wickert, J., 1992. Non-linear vibration of a traveling tensioned beam. International Journal of Non-Linear Mechanics 27 (3), 503 – 517.
URL http://www.sciencedirect.com/science/article/pii/002074629290016Z

[28] Yastrebov, V., 2013. Numerical Methods in Contact Mechanics. John Wiley & Sons, Ltd.

Journal Pre-proofs